J Therm Anal Calorim (2010) 102:953–959
DOI 10.1007/s10973-010-0801-1

Influence of additives on the thermal behavior of nickel/metal hydride battery

Kai Yang · Jin Jing An · Shi Chen

Received: 5 February 2010 / Accepted: 9 April 2010 / Published online: 6 May 2010

Abstract This study discusses the thermal behavior of the 6.5 Ah cylinder Ni/MH hydride battery with 0.5 wt% ytterbium oxide (Yb_2O_3) in nickel electrode and 1.0 wt% super absorbent polymer (SAP) in hydrogen-storage alloy (MH) electrode during charging to 150% of its rating capacity. Quantity of heat and heat generation rate of the battery during charging are studied by quartz frequency microcalorimeter. Heat generation curve is fitted into a function, and heat transport equation is solved. Using measured data, the internal temperature profiles at the terminal moment of charging at 1C, 3C, and 5C are simulated by FEM. Influence of Yb_2O_3 and SAP on the thermal behavior of Ni/MH battery is examined by the two-dimensional thermal model. Results show that addition of Yb_2O_3 and SAP can achieve substantial improvement for thermal behavior of Ni/MH battery at 1C,3C, and 5C charging.

Keywords Ni/MH battery · Ytterbium oxide · Super absorbent polymer · Thermal model

Introduction

Advanced nickel/metal hydride (Ni/MH) battery have found application in power tools, electric vehicles (EV) and hybrid electric vehicles (HEV) in the past several years [1]. Despite the emergence of lithium ion battery and portable fuel cells, due to their excellent power property and low environmental load, Ni/MH battery continue to attract much attention because almost all of the commercial HEV employ Ni/MH battery as the power battery [2–4]. To achieve the required capacity, a large-scale battery is necessary for EV and HEV applications. However, higher capacity and higher power lead battery to generate much heat and cause the low charge efficiency of nickel electrode and the corrosion of hydrogen-storage alloy (MH) electrode. As a consequence, the amount of electrolyte decreases and service life of the battery is shortened. In the mean time, the volume and weight in a vehicle are rather limited, so as the battery size increases, the ratio of heat cooling area to heat generating volume decreases, and as the charge and discharge current increases, more heat is generated [5]. The high temperature can heavily influence the performance of battery, particularly in large units. And the excessive temperature rise and steep temperature gradient within a battery could also result in the battery failure [6].

Thus, thermal model is regarded as an important target to evaluate Ni/MH battery, which can be used in different situations and different batteries by changing parameters about physical property, heat generation rate and environment [7]. Therefore, it is very important to study the thermal behavior of them. Modeling and simulation of the battery's thermal behavior are useful for obtaining information concerning whether or not excessive heat could be removed, or how the operating temperature can be controlled in an appropriate range [8–10]. Computational fluid dynamics (CFD) and finite element methods (FEM) are recommended for the investigation of the thermal system [11].

K. Yang · J. J. An · S. Chen (✉)
School of Chemical Engineering & Environment, Beijing Institute of Technology, Beijing 100081, China
e-mail: ykbit@126.com

K. Yang
Electrical Engineering Department, China Electric Power Research Institute, Beijing 100192, China

To date, it has been found that addition of rare earth oxides to the nickel electrode and the hydrogen-storage alloy electrode improves battery performance significantly [12]. The use of this technique has attained excellent charge efficiency in EV and HEV applications. Some thermal analysis about rare earth elements and electrode materials have been reported in the last years [13–15]. But little has been reported about the effect of them on the thermal behavior of batteries using model. Super absorbent polymers (SAP) are compounds that absorb water and swell into many times their original size and weight. The substance name of SAP is sodium polpacrylate (PAA-Na) and the molecular formula is $-[CH_2-CH(COONa)]_n-$. And it is used in soil to create a water reserve, which is near the rhizosphere zone and benefits agriculture. Moreover it is environmentally safe, as it is biodegradable [16, 17]. Recent research is focused on the new uses of SAP. Accordingly, one commercially available SAP named Rheogic to reduce the thermal effect of battery is evaluated in this study.

In this work, a two-dimensional mathematical model with FEM is presented for investigating the use of Yb_2O_3 and SAP in battery design and determining how they can influence thermal behavior of battery. The aim is to optimize battery design and construct a practical Ni/MH battery with small thermal effect as well as good high power performance.

Experimental

Before the experiment, three D-type cylindrical Ni/MH battery with a rated capacity of 6.5 Ah are prepared. Of all the battery, the additives are different and Rheogic is used as the SAP. And both the Yb_2O_3 and SAP are blended into the electrodes. The battery are added 0, 0.5, and 0.5 wt% Yb_2O_3 in nickel electrode and corresponding 0, 0, and 1.0 wt% SAP in MH electrode, separately. The battery numbers are A, B, and C, respectively. Some details are in Table 1. Under the conditions of the same attachment amount of active material on electrodes, the thermal behavior of battery with different additives is studied. The Yb_2O_3 and SAP in the alkaline environment are stable enough and both of them are not easy to be degraded in the electrodes upon charging-discharging processes.

A TRH-5D quartz crystal automatic microcalorimeter is used to test the temperature of battery during charging. Then the heat capacity of battery and the quantity of heat during charging and discharging are calculated automatically by this instrument. The tested battery is installed in a special device which protects the battery from short circuit, as shown in Fig. 1. The vacuum insulation unit is used in the host of the microcalorimeter, which retains the performance of thermal insulation at the optimum condition. A quartz frequency thermometer with temperature resolution of 0.00005 K and precision of 0.001 is used as a temperature collection system. The temperature is measured once in each 9.6 s. Before measuring, the microcalorimeter is calibrated by testing heat capacity and calorific value of benzoic acid, which guarantees the precision and accuracy in the experimental process.

Table 1 Some parameters of the tested battery

Parameters	A	B	C
Additives	Yb_2O_3 (0%)	Yb_2O_3 (0.5%)	Yb_2O_3 (0.5%)
	SAP (0%)	SAP (0%)	SAP (1.0%)
R, radius/m	0.0161	0.0161	0.0161
H, height/m	0.0605	0.0605	0.0605
R, internal resistance/mΩ	2.7797	2.7893	2.9426
M, mass/g	176.77	178.89	178.46
V, volume/m^3	0.000049267	0.000049267	0.000049267
A, surface area/m^2	0.00769	0.00769	0.00769

In charging experiments, the Ni/MH battery is discharged to the cut-off voltage 1.0 V first. Then the battery is subsequently charged in 1C, 3C, and 5C rate to 150% of its rated capacity. The discharging and charging process is controlled by an Arbin instrument, and data are saved by the program on a personal computer. With these measured data, the internal temperature profile of the battery during charging is calculated by the thermal behavior model. In the mean time, heat generation rate can also be fitted into a function.

Results and discussion

Model description

In general, a thermal model is typically formulated based on the thermal energy balance over a representative

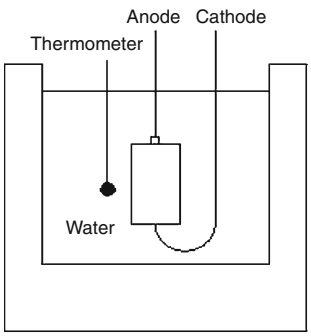

Fig. 1 Experimental device system

elementary volume in a battery. For most battery systems, the convection term could generally be neglected. The battery is assumed to be axial symmetric. And density, thermal conductivity and heat capacity of the battery are assumed to remain constant within a certain temperature range. Based on these assumptions, the following transient partial differential equation Eq. 1 is sufficient to describe the temperature profile in the cylindrical battery. The initial and boundary conditions are shown in Eqs. 2 and 3.

$$\mathrm{MC_p}\frac{\partial T}{\partial t} = V\frac{1}{r}\frac{\partial}{\partial r}\left(\kappa_r r\frac{\partial T}{\partial r}\right) + V\frac{\partial}{\partial z}\left(\kappa_z\frac{\partial T}{\partial z}\right) + Q \tag{1}$$

$$\text{IC: } T(r,z,0) = T_0 \tag{2}$$

$$\text{BC: } -\kappa_r\frac{\partial T}{\partial r}\Big|_{r=R} = \alpha\left(T|_{r=R} - T_\infty\right),\ -\kappa_z\frac{\partial T}{\partial z}\Big|_{z=0,H} = \alpha\left(T|_{z=0,H} - T_\infty\right) \tag{3}$$

C_p is average heat capacity, which is measured by the microcalorimeter before charging and assumed constant; k_r and k_z are, respectively, the thermal conductivities of the battery in r-direction and z-direction, which can be accessed through references, T_0 denotes the initial temperature of the battery, which has the same value with the temperature measured by microcalorimeter; Q is heat generation rate, α denotes heat transfer coefficient, T_∞ is ambient temperature. The values are shown in Table 2. And the parameters used in the thermal modeling of battery are listed in Tables 1 and 2.

Experiment results

In a normal charging process, the battery reaction heat, electrochemical polarization heat and joule heat are sources of heat generation, and battery reaction heat is a dominant factor. When the battery is overcharged, the battery reaction heat equals zero and sub-reactions occurs, which causes the generation of sub-reaction heat. And the sub-reactions in the positive electrode and negative electrode are shown in (4) and (5), respectively.

$$\text{In the positive electrode : } \quad 2OH^- \rightarrow H_2O + \frac{1}{2}O_2 + 2e \tag{4}$$

$$\text{In the negative electrode: } \quad H_2O + \frac{1}{2}O_2 + 2e \rightarrow 2OH^- \tag{5}$$

The test results show that there is little difference among the resistance of battery with different additives, which are concentrated distribution in 2.7 ~ 2.9 mΩ. Quantity of heat and temperature rise during charging at 1C, 3C, and 5C are measured by quartz frequency microcalorimeter and the results are shown in Table 3. The relationships between quantity of heat, temperature rise, and battery number are, respectively, shown in Figs. 2 and 3. It can be seen that the change tendency of them is consistent with each other. That is to say, quantity of heat and temperature rise decrease gradually from A, B to C, which initially means that the battery with 0.5 wt% Yb_2O_3 in nickel electrode and 1.0 wt% SAP in MH electrode generates less heat than others.

During charging, heat generation rate (Q) changes with time (t). Battery A is taken for example, curves of heat generation rate during charging at 1C, 3C, and 5C are shown in Fig. 4. During normal charging, joule heat is a significant factor in this period and heat generation rate is small. At the beginning of 3C and 5C, the heat generation rate rises more rapidly than 1C; after a period of time, heat generation rate increases slightly, and the rate of Q decreases. During overcharging, oxygen generated at the positive electrode reacts with hydrogen at the negative electrode to form water, thus heat generation rate is higher than that of the normal charging process. Accordingly, the heat generation rate increases rapidly, and curves become much steeper and can be fitted into exponential functions. Take A for example, heat generation rate of 1C, 3C, and 5C could be expressed by Eqs. 6, 7, and 8, respectively.

$$\text{For 1C : } \quad Q = \begin{cases} 0.44135 + 0.00017247t, 0 < t \le 3225.6 \\ 9.11029 - 8490.15207 \times 0.99792^t, 3225.6 < t \le 5400 \end{cases} \tag{6}$$

$$\text{For 3C : } \quad Q = \begin{cases} 1.86007 + 0.00304t, 0 < t \le 1056 \\ 41.50936 - 211.71188 \times 0.99841^t, 1056 < t \le 1800 \end{cases} \tag{7}$$

$$\text{For 5C : } \quad Q = \begin{cases} 3.25774 + 0.01063t, 0 < t \le 614.4 \\ 399.1316 - 455.41029 \times 0.99975^t, 614.4 < t \le 1080 \end{cases} \tag{8}$$

T_∞ is estimated by Eq. 9. T_max is the maximum temperature during charging, and Time represents the measured time

Table 2 Values of parameters in thermal model

Parameters	A	B	C
C_p, heat capacity/J kg^{-1} K^{-1}	250.2139	225.7014	214.1139
κ_r, thermal conductivity in r-direction/J s^{-1} m^{-1} K^{-1}	0.74 [1]	0.74 1	0.74 [1]
κ_z, thermal conductivity in z-direction/J s^{-1} m^{-1} K^{-1}	0.85 [1]	0.85 [1]	0.85 [1]
T_0, initial temperature/K	293.15	293.15	293.15

Table 3 Quantity of heat and temperature rise during charging at 1C, 3C and 5C

	Parameters	A	B	C
1C	Q_h, quantity of heat/J	12937.03	12353.80	11447.79
	ΔT, temperature rise/K	2.42503	2.35379	2.27208
3C	Q_h, quantity of heat/J	17920.42	17218.05	16728.36
	ΔT, temperature rise/K	2.80866	2.67673	2.54641
5C	Q_h, quantity of heat/J	21200.69	20982.14	20057.81
	ΔT, temperature rise/K	3.23042	3.08333	2.97641

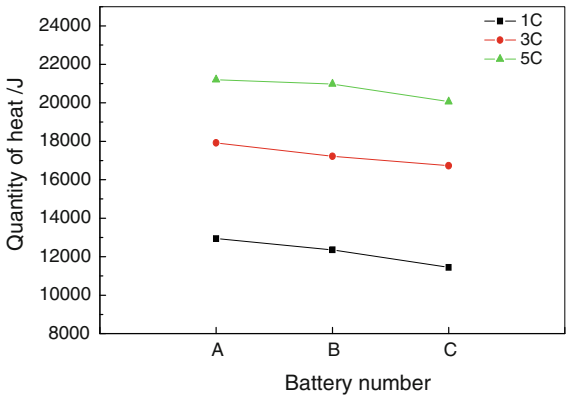

Fig. 2 Quantity of heat during charging at 1C, 3C, and 5C

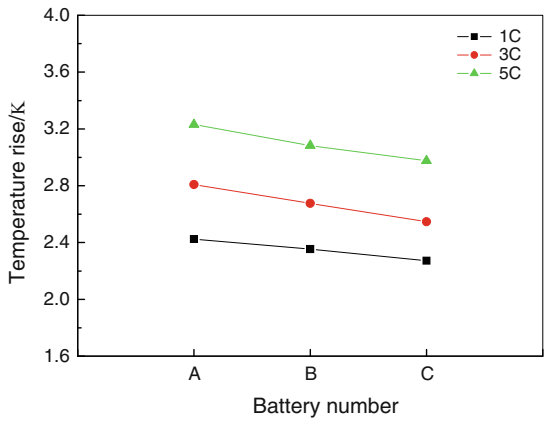

Fig. 3 Temperature rise during charging at 1C, 3C, and 5C

from the initial temperature to the maximum temperature. For charging at 1C, 3C, and 5C, the ambient temperature of A, B, and C are shown in Eqs. 10–12, 13–15, and 16–18, respectively.

$$T_\infty(t) = 20.00 + (T_{\max} - 20.00) \times t/\text{Time} \quad (9)$$

$$\text{For 1C}: T_\infty = 293.15 + 0.00042388t \quad (10)$$

$$T_\infty = 293.15 + 0.00041940t \quad (11)$$

$$T_\infty = 293.15 + 0.00039700t \quad (12)$$

$$\text{For 3C}: T_\infty = 293.15 + 0.00127200t \quad (13)$$

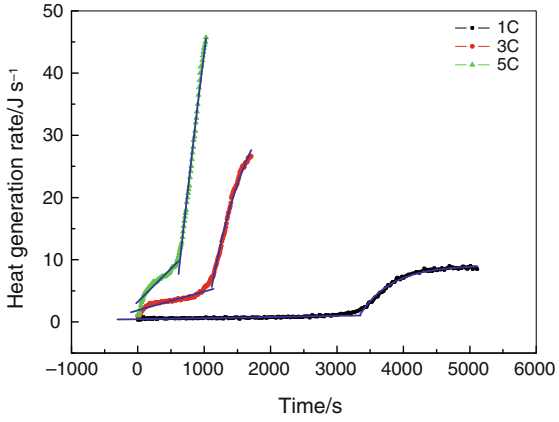

Fig. 4 Heat generation rate during charging at 1C, 3C, and 5C of battery A

$$T_\infty = 293.15 + 0.00121200t \quad (14)$$

$$T_\infty = 293.15 + 0.00120200t \quad (15)$$

$$\text{For 5C}: T_\infty = 293.15 + 0.00196800t \quad (16)$$

$$T_\infty = 293.15 + 0.00204800t \quad (17)$$

$$T_\infty = 293.15 + 0.00215700t \quad (18)$$

According to Newton's law of cooling, heat transfer coefficient (α) is expressed by Eq. 19. Q_{dis} represents heat dissipation rate. A represents the battery surface area, which is shown in Table 1. ΔT denotes temperature difference between battery wall and ambient temperature. The experiment shows that ΔT is smaller than 3 K, so we assume it to be constantly 3 K for simplicity. During charging, the heat dissipation rate changes with time, which can be considered as heat generation rate.

$$\alpha = Q_{dis}/A\Delta T \quad (19)$$

Solutions of Eqs. 1–3 are shown in Figs. 5, 6, and 7, two-dimensional temperature profile in the r-direction and z-direction at the terminal moment of 1C, 3C, and 5C rate charging. The temperature distribution inside the battery is non-uniform because of the poor heat conductivity of the materials used in the battery. Therefore, high rate charging and discharging for a long time should be avoided in practical use. The central temperature simulated by FEM is shown in Fig. 8. For battery C, the temperature profiles of 1C, 3C, and 5C rate charging are lower than other battery.

It is well known that the combination of oxygen generating from nickel electrode occurs on MH electrode when Ni/MH battery is overcharged, which intensifies the generation of heat. And the oxygen overpotential of nickel electrode drops rapidly in the high-temperature range of over 308.15 K, which also causes the charge efficiency to decrease owing to the charging reaction and the oxygen

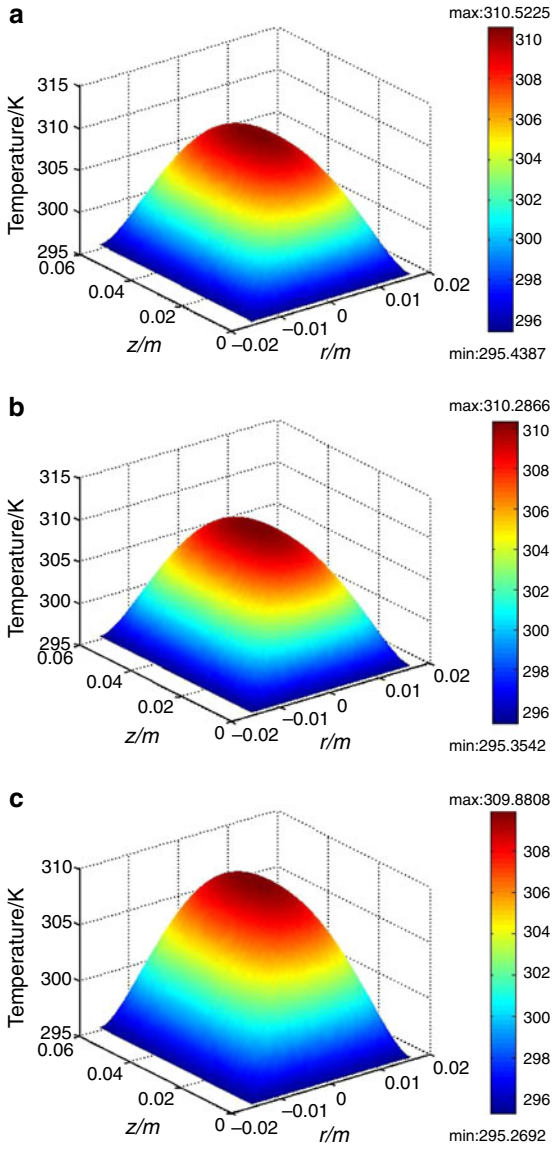

Fig. 5 Temperature distribution of A (**a**), B (**b**), and C (**c**) at the terminal moment of charging at 1C

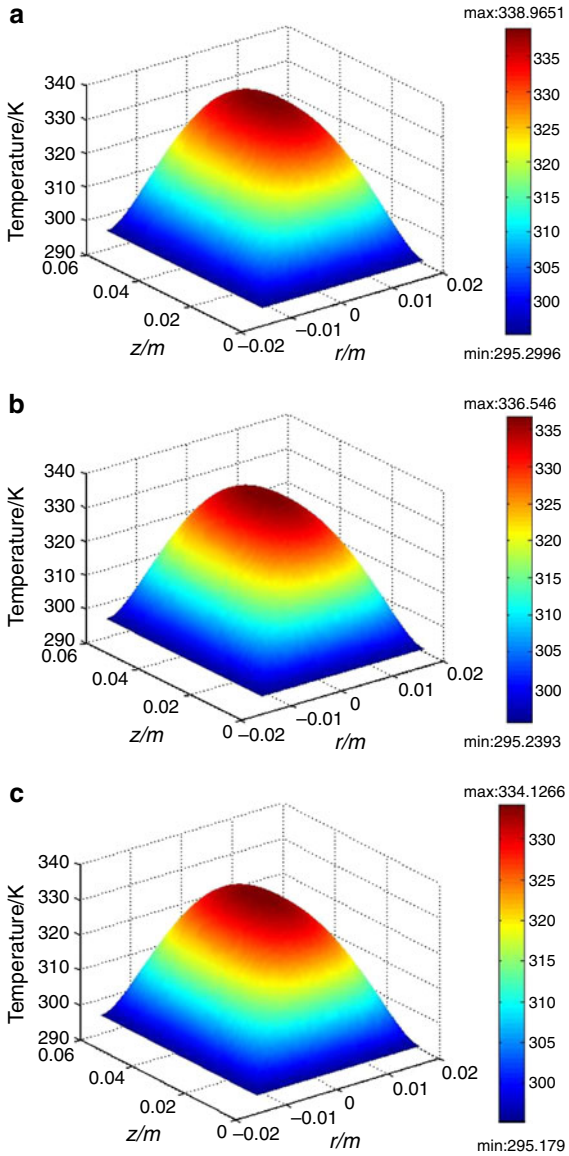

Fig. 6 Temperature distribution of A (**a**), B (**b**), and C (**c**) at the terminal moment of charging at 3C

evolution reaction conflicting with one another. Therefore, increasing oxygen overpotential is an effective method to reduce the thermal behavior of Ni/MH battery. Since the addition raises the charge efficiency of battery, it is considered to suppress oxygen evolution in the final charging stage, which in turn restrains the corrosion of MH electrode caused by oxygen. Compared with A, battery B is added 0.5 wt% Yb_2O_3 in positive electrode. Battery A without Yb_2O_3 has smaller capacity stemming from declining charge efficiency in the final charging stage. The maximum internal temperature of B is, respectively, 0.235, 2.419, and 3.062 °C less than A at the terminal moment during charging at 1C, 3C, and 5C, which shows that Yb_2O_3 contributes to generate less heat and cause a more uniform temperature profile. The reason is the oxygen evolution overpotential of nickel electrode is raised resulting from the addition of Yb_2O_3. It also seems that Yb with many electrons in 4f orbital is very effective for increasing the hydrogen overpotential. The increased hydrogen overpotential delays the evolution of hydrogen from MH electrode and holds down the buildup of the pressure of the battery. In the mean time, the addition of Yb_2O_3 to nickel electrode is effective for improving capacity-retention characteristics and mitigating autolysis of the nickel electrode and their reduction.

Compared with B, battery C is added 1.0 wt% SAP in negative electrode. The maximum internal temperature of C is, respectively, 0.406, 2.419, and 3.061 K less than B at

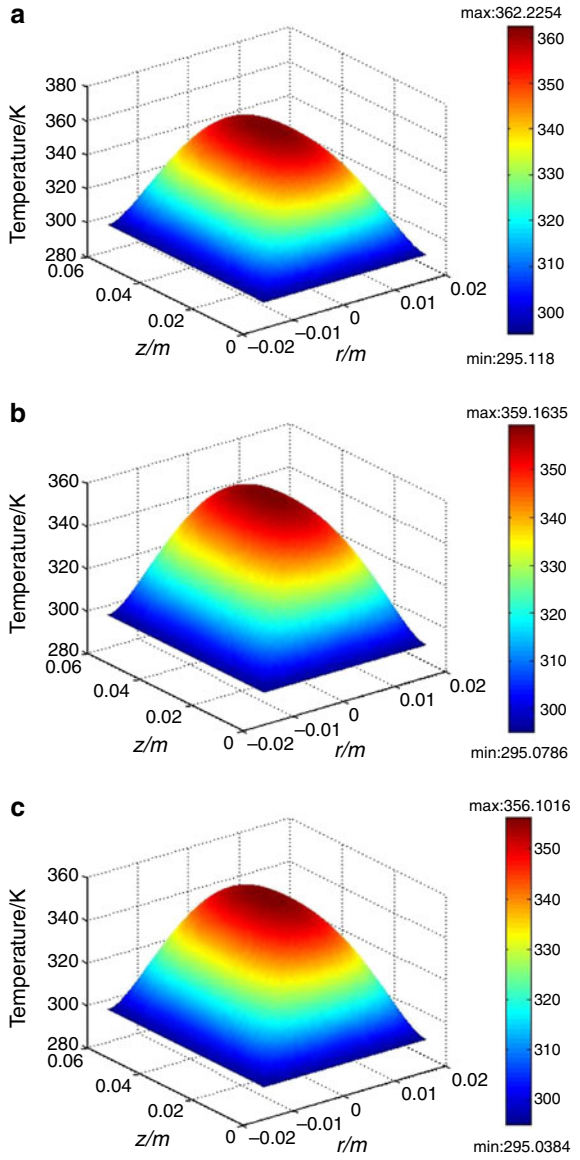

Fig. 7 Temperature distribution of A (**a**), B (**b**), and C (**c**) at the terminal moment of charging at 5C

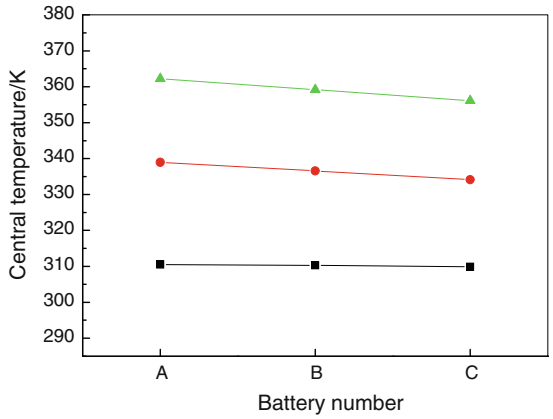

Fig. 8 The central temperature during charging at 1C, 3C, and 5C

Table 4 Comparison of experiment and simulation surface temperature rise

Rate	Temperature/K	A	B	C
1C	Experiment	2.399	2.335	2.250
	Simulation	2.289	2.204	2.119
3C	Experiment	2.487	2.401	2.373
	Simulation	2.150	2.089	2.029
5C	Experiment	2.537	2.432	2.343
	Simulation	1.968	1.929	1.888

the terminal moment during charging at 1C, 3C, and 5C, which shows that C generates less heat and has a more uniform temperature profile. SAP can absorb water of 200–1000 times of its weight [18]. Accordingly, addition of Rheogic as SAP in MH electrode can slow the water evaporation, keep electrolyte well distributed in electrode and decrease pulverization and peeling phenomena, which make active materials distribute more uniform. Therefore, electrons transfer more unobstructed and polarization potential decreases due to the forming of an excellent conductive network. Consequently, less heat is generated during charging at large currents for battery C.

The surface temperature rise by experiment and simulation are shown in Table 4. Comparing with the results of experiment, simulation results are lower than actual rises. It seems that the cooling efficiency has been overestimated possibly owing to the estimation of a. The experiment value is the temperature of measurement position which is not on the battery surface but in the ambient environment close to the battery. However, the difference is very small. After charging, the battery no longer generates heat and accumulated heat spreads to the environment gradually. The internal heat of the battery tends to be in equilibrium with the environment, which makes the difference between the simulation temperature and the experimental values decrease. The temperature rises are close especially for 1C charging, therefore, the results using the simulation method are comparatively accurate.

Conclusions

In this study, the effects of Yb_2O_3 and SAP on the thermal behavior of 6.5 Ah Ni/MH battery during charging at 1C, 3C, and 5C are discussed. Quantity of heat and heat generation rate of the batteries are studied by quartz frequency microcalorimeter. Heat generation rate could be fitted into functions. Using measured data, the internal temperature profiles at the terminal moment of charging are simulated by FEM. For all the charging currents, the thermal behavior of the battery with 0.5 wt% Yb_2O_3 in nickel electrode and

1.0 wt% SAP in MH electrode always keeps the minimum. Therefore, addition of Yb_2O_3 and SAP is effective in improving the performance of Ni/MH battery and they are recommended in the design of the battery.

Acknowledgments This work is supported by the National Key Basic Research and Development Program of China (Grant No. 2009CB220100).

References

1. Wu MS, Wang YY, Wan CC. Thermal behaviour of nickel/metal hydride battery during charge and discharge. J Power Sources. 1998;74:202–10.
2. Taniguchi A, Fujioka N, Ikoma M, Ohta A. Development of nickel/metal-hydride batteries for EVs and HEVs. J Power Sources. 2001;100:117–24.
3. Ying TK, Gao XP, Hu WK, Wu F, Noreus D. Studies on rechargeable Ni/MH batteries. Int J Hydrog Energy. 2006; 31:525–30.
4. Soria ML, Chacon J, Hernandez JC, Moreno D, Ojeda A. Nickel metal hydride batteries for high power applications. J Power Sources. 2001;96:68–75.
5. Onda K, Ohshima T, Nakayama M, Fukuda K, Arakia T. Thermal behavior of small lithium-ion battery during rapid charge and discharge cycles. J Power Sources. 2006;158:535–42.
6. Shi J, Wu F, Chen S, Zhang C. Thermal analysis of rapid charging nickel/metal hydride battery. J Power Sources. 2006; 157:592–9.
7. Yang K, Li DH, Chen S, Wu F. Thermal behavior of nickel/metal hydride battery during charging and discharging. J Therm Anal Calorim. 2009;95:455–9.
8. Freitas GC, Peixoto FC, Vianna AS. Simulation of a thermal battery using Phoenics. J Power Sources. 2008;179:424–9.
9. Chen SC, Wan CC, Wang YY. Thermal analysis of lithium-ion batteries. J Power Sources. 2005;140:111–24.
10. Li D, Yang K, Chen S, Wu F. Thermal behavior of overcharged nickel/metal hydride Battery. J Power Sources. 2008;184:622–6.
11. Liaw BY, Bethune KP, Yang XG. Advanced integrated battery testing and simulation. J Power Sources. 2002;110:330–40.
12. Tanaka T, Kuzuhara M, Watada M, Oshitani M. Effect of rare earth oxide additives on the performance of Ni/MH batteries. J Alloys Compd. 2006;408–412:323–6.
13. Sroda M. Effect of Er_2O_3 on thermal stability of oxyfluoride glass. J Therm Anal Calorim. 2009;97:239–43.
14. Ito A, Tanaka K, Kawaji H, Atake T, Ando N, Hato Y. Magnetic phase transition of $Li_{0.75}CoO_2$ compared with $LiCoO_2$ and $Li_{0.5}CoO_2$. J Therm Anal Calorim. 2008;92:399–401.
15. Gorzkowska I, Jozwiak P, Garbarczyk JE, Wasiucionek M, Julien CM. Studies on glass transition of lithium-iron phosphate glasses. J Therm Anal Calorim. 2008;93:159–62.
16. Davies LC, Novais JM, Martins-Dias S. Detoxification of olive mill wastewater using superabsorbent polymers. Environ Technol. 2004;25:89–100.
17. Dhodapkar R, Rao NN, Pande SP, Nandy T, Devotta S. Adsorption of cationic dyes on Jalshakti, super absorbent polymer and photocatalytic regeneration of the adsorbent. React Funct Polym. 2007;67:540–8.
18. Jina ZF, Asakob Y, Yamaguchib Y, Yoshidab H. Thermal and water storage characteristics of super-absorbent polymer gel which absorbed aqueous solution of calcium chloride. Int J Heat Mass Transf. 2000;43:3407–15.